X-651-64-132

TM X-55047

EXAMPLES OF CERTAIN DATA REDUCTION AND MAPPING PROCEDURES UTILIZING TIROS III FIVE-CHANNEL RADIOMETER DATA

APRIL 30, 1964

NASA GODDARD SPACE FLIGHT CENTER

GREENBELT, MARYLAND

"Examples of Certain Data Reduction and Mapping Procedures Utilizing TIROS III Five-Channel Radiometer Data"

Lewis J. Allison
Goddard Space Flight Center

Guenter Warnecke*
Goddard Space Flight Center

April 30, 1964

*On leave from the Institut für Meteorologie und Geophysik der Freien Universitat Berlin; Berlin, Germany as National Academy of Sciences-National Research Council Research Associate with the National Aeronautics and Space Administration.

ABSTRACT

Selected examples of current data reduction and mapping procedures are discussed for the purpose of demonstrating their utility as well as their limitations.

INTRODUCTION

In order to analyze and accurately interpret the TIROS radiation data, certain data reduction and mapping processes are described which should be of interest to the researcher and meteorologist alike.

A brief description of the 5-channel scanning radiometer is included for the benefit of the reader who may be unfamiliar with the TIROS radiation experiment.

1. THE FIVE CHANNEL SCANNING RADIOMETER

The TIROS III scanning radiometer consists of a five-channel instrument. The five channels are sensitive in the following spectral regions:[1]

Channel	Spectral Region	
1	6.0 to 6.5μ	(radiation within the ν_2 fundamental water vapor band)
2	8 to 12μ	(radiation emitted in the atmospheric "window")
3	0.2 to 6μ	(total reflected solar radiation (albedo))
4	8 to 30μ	(total infrared radiation of the earth-atmosphere system)
5	0.55 to 0.75μ	(reflected solar radiation within the visible part of the spectrum)

The 5-channel radiometer employs a chopper that causes each sensor to view alternately and at a rapid rate, in two directions 180 degrees apart. At least one direction always views outer space which serves as a zero radiation reference. The response from each channel is proportional to the difference in the irradiation of the sensor bolometer from the two directions. When both optics view outer space, the resultant signal is designated as the "space viewed level". The bi-directional axes

of the channels are parallel to one another and inclined to the spin axis by 45 degrees (Figure 1).[2]

2. REMARKS ON THE DATA REDUCTION AND MAPPING PROCEDURES

2.1 Equivalent Blackbody Temperature

The calibration of the infrared channels is in terms of equivalent temperatures, T_{BB}, of a blackbody target filling the 5° field of view, whereas the calibration of the solar channels is in terms of that portion of radiant emittance from a target filling the field of view to which the channel responds through its filters and other optical elements.[2]

The family of curves of equivalent blackbody temperatures vs effective radiant emittance for TIROS III (Figure 2), were obtained by integrating the Planck function over the spectral response curves for Channels 1, 2 and 4.[1,3] The estimated relative accuracy of equivalent blackbody temperature for Channels 1, 2 and 4 is $\pm 2^{\circ}K$, while the estimated absolute accuracy is $\pm 4^{\circ}$ to $\pm 8^{\circ}K$, up to orbits 118, 875 and 130 respectively, after which degradation of the instrumental response becomes appreciable.[1,4]

A degradation correction nomogram for Channel 2 measurements (Figure 3), based upon degradation models inferred from the relevant data obtained by the respective radiometer has been included.[4] The nomogram was developed from a computer program which determined the time rate of change of the measured total emitted radiant power between latitudes 55°N-55°S. The results showed that Channel 2 degraded continuously following the TIROS III launch. The degradation for Channel 2 was determined to be symmetrical, i.e., independent of the side (wall or floor aperture) of the

satellite. The nomogram (Figure 3) may be used with some degree of confidence up through orbit 875. Beyond this subjectively determined limiting orbit, the correction nomogram becomes correspondingly uncertain. A more detailed discussion of the factors effecting the response of the scanning radiometer may be found in Reference 5.

2.2 The Radiation Data Processing Procedure

The medium resolution radiometer data that are recorded at the read-out station are demultiplexed, demodulated and fed to an analog-to-digital converter at the Goddard Space Flight Center.[2] This converter produces a magnetic "Radiation Data Tape" made up of 36 bit words suitable for an IBM 7094 computer. Analog records may be produced on a recording oscillograph for special hand analysis. The computer produces a Final Meteorological Radiation Tape (FMRT) when combined with the inputs from the Radiation Data Tape, Orbital Tape and Calibration. The most convenient method of presentation of these FMRT data is to make grid print maps from an IBM 7094 computer. Several problems arising in the composition and averaging of the original radiation data are discussed below.

2.3 Radiation Data Resolution

The data resolution of computer produced radiation maps, printed on a mercator map base is directly affected by the following:

2.3.1 Nadir Angle Variation

Radiation data contained on the FMR Tapes are sampled approximately 8 times per second. Thus, at the nominal 10 rpm spin rate, approximately 48 samples are taken during each satellite rotation. Data sampled during the earth-

viewed portion of the scan having the smallest nadir angle will be the most densely located, with progressively greater separation occurring at the higher nadir angles. Additionally, the size of the scan spot varies considerably with the nadir angle and with the height of the satellite. For example, at an 800 km satellite height (Figure 4) the elongated scan spot resolved by the radiometer at a 56.6° scan nadir angle, would enclose approximately 10 times the scan spot area at a scan nadir angle of zero.[6] Thus the higher the radiometer nadir angle, the lower the data resolution.

Figure 5 shows that the nominal 5 degree field of view of the radiometer pertains to the 50% of peak-response level, and that there is some residual response to about ±4 degrees from the optical axis.[7] The percent power scan spots of Figure 4 are directly derived from this response curve.

2.3.2 Grid Print Map Scale

The mesh size of the multi-resolution mercator mapping program is 0.5 inches. Thus, the number of degrees of longitude per mesh interval is in effect the selection of the map scale. A resolution of 0.625°, 1.25° and 2.50° of longitude per mesh interval corresponds to a map scale of approximately 1:5 million, 1:10 million and 1:20 million, respectively, near the equator. On a mercator projection the map scale increases with increasing latitude. The larger the map scale, the higher the resolution, the lower the number of measurements averaged within the 1/2 inch area around each grid point.

In order to illustrate the effect of map scale on data resolution, several TIROS III television pictures

and radiation charts are shown in the following. The well-defined cloud system at 10°N, 40°W on July 16, 1961, which was identified by S. Fritz[8] as being the cloud mass from which Hurricane ANNA, later developed in July, 1961, was selected as the example.

Figure 6a shows the "window" radiation analysis based upon hand-plotted data from a computer listing, which contains the geographical location, the nadir and azimuth angles, and the simultaneous readings of all five radiation channels for every single scan spot. The location of each scan spot is indicated by a cross in Figure 6a. This is the most detailed information available from the FMR Tape.

Figure 6b is a composite of the "window" radiation field shown in the previous figure and the gridded TIROS photograph of the same area. The latitude-longitude grid of this picture was obtained from a computer program.

The agreement between the picture information and the radiation field in the "window" region is surprisingly good, even at the fringes of the photograph. Considering the range of accuracy of satellite attitude determination and the computer gridding programs, it is interesting to note that the radiation data fit the television pictures within one degree of latitude and longitude. An equivalent blackbody temperature difference of more than 50°K was indicated between the cloudless area and the highest cloud tops.

A similar radiation analysis (Figure 6c) was later performed by L. F. Whitney, Jr. of the National Weather Satellite Center, U.S. Weather Bureau, using the highly accurate

Fujita method.[6] This method employs analog records produced on a recording oscillograph for special hand analysis rather than the automatically processed FMR Tapes. It should be considered, however, that this picture represents another frame of the same series, one minute later in time. From Figures 6b and 6c one can judge, that, at least in this case, the evaluation of the FMRT data does not result in any significant loss of details when compared with the results of the Fujita technique.

Figure 7 shows the radiation analysis of the same storm area based on three different types of computer produced grid maps at three different grid spacings, viz., 0.625^{o}, 1.25^{o}, and 2.50^{o} longitude per mesh interval, corresponding to approximate map scale of 1:5 million, 1:10 million and 1:20 million respectively. The data points are again indicated in each figure. From the left to the right it becomes clear that the appropriate selection of the map scale for each radiation study is of great importance, as detailed in the isoline configuration and extreme values of equivalent blackbody temperatures become "washed out" by the averaging processes involved at smaller map scales. Thus, for the analysis of more detailed synoptic features, a grid spacing of 0.625^{o} of longitude per mesh interval is the most useful one, but the accuracy in data location is considerably less than by use of hand-plotted maps of the FMRT computer listings and of maps produced by the more precise Fujita method. Grid spacings of 2.50^{o} longitude and 1.25^{o} of longitude/mesh interval are also possible and resolve many details, but the size of these computer prints becomes rather unhandy.

2.4 Radiometer Scanning Modes

Figure 1 showed the basic relationships between the satellite's spin axis and the radiometer axis.

As the satellite rotates on its axis, the radiometer scan pattern is defined by the intersection of a 45° half-angle cone and the earth. This pattern ranges from nearly a circle (closed mode) when the satellite nadir angle is less than 17°, to two hyperbola-like branches in the "wall" and "floor" directions, when the spin vector is approximately perpendicular to the orbital radius vector.[1]

Therefore the three patterns of earth scanning modes, (Figure 8) can be distinguished as follows.[9]

1) Single Open Mode: Some scan spots of a spin cycle are space viewed and the remainder are earth viewed through the wall (side) sensor only or through the floor (baseplate) sensor only.
2) Closed Mode: All the scan spots throughout a number of spin cycles of the satellite are earth-viewed, either through the wall or the floor sensor.
3) Alternating Open Mode: The scan spots of a spin cycle are alternately viewed through the wall sensor and the floor sensor.

The IBM 7094 computer can easily be programmed to distinguish between different modes and to use or omit certain scanning modes. For example, in Figure 9 for orbits 56 and 58, those parts with single open mode data are grey shaded,

and it is obvious that large and important parts of the data coverage are lost if closed mode data are omitted. Some examples of actual scan lines and scan spots are indicated on orbit 56. Additionally in this figure, the computer grid print map of orbit 57 is introduced, showing the full data coverage along the orbital path. However, there is a significant difference in accuracy of the geographical location between open and closed mode data, which reduces the applicability of closed mode data unless a very detailed investigation of possible short-term aberrations of the pseudo-spin rate value used in the computer reduction of the closed mode data is performed for every individual case. In the following sections these practical difficulties will be discussed more in detail.

An example of typical closed mode data mislocation is given in Figure 10. This figure includes 10 minutes of closed mode data and shows the radiation "cloud" pattern of the early stage of Hurricane Anna at the same location within minutes of the same time as shown in Figure 7, which included open mode data only. This longer time period permitted the complemental scans of the closed mode to follow by several minutes the initial scans through the storm area (see Figure 8), resulting in an apparent shift of data leading to the ficticious cold (high cloud) area in the SW quadrant of the figure. The floor aperture of the satellite was viewing the storm at this time, and a 6 scan spot shift in a counterclockwise direction was confirmed by diagnostic methods. The computer program averaged the displaced scan spot data with the preceding accurately positioned open mode scan spots and presented and erroneously elongated cloud structure.

A separate example of analog presentations of open and closed mode patterns is shown in Figures 11 and 12. Line A identifies the measurement obtained when viewing the perinadir in an open mode swath. This line is centered between the horizons of the swath and all the scan spots are positioned symmetrically about this line by the computer program, in accordance with the spin rate. Normally there can be little or no error in positioning these scan spots since each swath is processed individually and the horizons for each are determined quite accurately. For the closed mode swaths, mislocation errors do occur simply because there are no horizons detected by the satellite and the location of the data must be determined solely by the spin rate.

The spin rate used in the data reduction program is measured by means of counting cycles of a standard clock at the read-out station between sun pulses and is assumed to be constant throughout the closed mode. For a spin rate determination error of 0.01^{o}/sec (or 1 part in 6000), the spin angle error at the end of 10 minutes would be 6^{o}, or about equal to one scan spot.[9]

The computer program is such that the first scan spot (Spot B) after the last open mode swath is positioned on the aponadir (Spot B'), a shift backward of 2 1/2 scan points or about 15^{o} of the spin angle.

All succeeding scan spots in the swath are shifted proportionally which results in a shift of the radiation data by 2 1/2 scan spots (approx. 200 km). Figure 13 illustrates this mislocation in relation to geographic position, giving, however, examples for points close to center of the swaths. The measurement at point H of the first closed mode swath, which should be contiguous to that of point G within the last open mode swath, will be mislocated by the computer and appears in the wrong position H'. Comparing the last closed with the first open mode swath, point I should be contiguous to the measurement at point J; in this instance however, it was mislocated by the computer and shifted into the wrong location I'.

The 1 1/2 to 2 1/2 scan spot shift that occurs at the beginning of the closed mode is always counter to the rotation of the swath. If the spin rate used in the computer program is less than the actual rate, the mislocation of successive scan spots will be counter to the scan rotation. If the assumed spin rate is greater than the actual, the mislocation will be in the direction of the scan rotation.

The spin rate used for the 7 orbits in this study were all less than the actual rate, so that by the end of the closed mode, the mislocation averaged six data points or about 36^{o} of the spin angle counter to the direction of scan rotation. Therefore, all scan spots were shifted backwards so that by the end, they were 6 spots too far in back of the true position. Thus, for example, spot C' was erroneously located on the aponadir, (Figure 12) instead of on its correct position which should have been 6 spots ahead of the aponadir.

In order to improve the accuracy of location of the closed mode data, steps have been initiated to calculate the pseudo-spin rate values which should be individually applied to each closed mode sequence in the automatic reduction of the data.

2.5 Measurements Falling Below the Space-earth Discriminant

For the reasonable interpretation of the recorded radiometer signals it is necessary to distinguish very carefully between earth-scanned data and space-viewed or space-contaminated data. Therefore, the computer logic was set to make the distinction by means of an arbitrarily defined threshold value below which the data should be defined as "space viewed". Theoretically, this space-earth discriminant should be identical with the space viewed level and be located far from all atmospheric data. Practically, however, it is necessary to define the threshold value above the noise level of the radiometer system. Normally, there is no interference with real atmospheric measurements. But in the case of very low radiation intensities the actual equivalent blackbody temperatures may be lower than the threshold value. This occurs mainly over areas of very high opaque cloud systems such as tropical storms.

If a measurement appears below the space-earth discriminant, according to the TIROS III Radiation Data Users' Manual [1], it will be flagged by a minus sign on the FMR Tape and in the computer listings. Three or more consecutive values below the threshold will be assumed to be the end of an open mode swath by the computer logic (i.e., when the satellite nadir angle is larger than about 17 degrees, the exact value depending upon the satellite height). Also, all data making up the terminal swath of the closed mode are flagged with minus signs for

diagnostic purposes. This means that over large high-cloud areas or when an unusually high noise level occurs just in the transition between closed and open scanning modes, the computer logic may not be able to distinguish properly between real earth-scanned and space-viewed data, resulting in a large number of measurements being flagged with minus signs.

Generally, the computer will be ordered to reject all data flagged by a minus sign in order to avoid the use of questionable data. The computer has, however, an option to accept these data for grid print maps. Therefore, a careful check of the FMR Tape data is necessary under such circumstances to permit the analyst in advance to select the areas where the flagged data are meaningful for mapping.

An example of such an occurrence is given in Figure 14. By inspecting the population count, which shows how many data points are contributing to each grid point in the computer produced grid print map, for orbit 62 an irregularity is noted over the Philippine Islands. Approximately 20 data points were rejected by the computer in every grid square in this area. Figure 15 shows all the single data points taken from the computer listings. All data accepted by the computer mapping program are marked by a rectangle, while the rejected "flagged" data points are encircled. The final (Figure 16) analysis of this radiation field shows that just the most interesting low radiation temperature data (very high reaching dense cloud system) over Tropical Storm Flossie had been rejected. Thus, the effect of the artifically defined space-earth discriminate on the composition of radiation data over certain meteorologically

significant areas should always be accounted for in detailed studies. In certain cases, perhaps, the space-earth discriminate could be set somewhat lower, but this depends on such condition of signal-to-noise ratio, radiometer housing temperature, etc. which are discussed in Reference 10.

28088

3. CONCLUSIONS

This paper has attempted to review briefly the satellite radiation experiment and to discuss the current TIROS radiation data reduction processes. With improvement and modification of the computer processing procedures, it will become possible to reduce the location (closed mode) uncertainties of the data and also to accept low but real measurements so that these data could be used in operational weather analyses.

Author

REFERENCES

1. TIROS III Radiation Data Users' Manual, Goddard Space Flight Center, NASA, August 1962.

2. W. R. Bandeen, "Data Processing From Meteorological Satellites," NASA SP-16, Nat'l. Aero. and Space Admin., Dec. 1962.

3. Nordberg, W., W. R. Bandeen, B. J. Conrath, V. Kunde, and I. Persano, "Preliminary Results of Radiation Measurements from the TIROS III Meteorological Satellite", Jrl. Atmosp. Sci., 19, 20-30, 1962.

4. W. R. Bandeen, R. E. Samuelson, I. P. Strange, "TIROS III Radiation Data Users' Manual Supplement, Correction Models for Instrumental Response Degradation," NASA, Goddard Space Flight Center, Dec. 1, 1963.

5. W. R. Bandeen, V. Kunde, W. Nordberg, and H.P. Thompson, "TIROS III Meteorological Satellite Radiation Observations of a Tropical Hurricane", Tellus - to be published (1964).

6. Fujita, T. "Outline of a Theory and Examples for Precise Analysis of Satellite Radiation Data", Research Paper 15, University of Chicago, Feb. 1963.

7. Astheimer, R. W., "De Waard, R. and Jackson, E. A. "Infrared Radiometric Instruments on TIROS II", Jrl. of Optical Society, 51, 1386-93, Dec. 1961.

8. Fritz, S., "Satellite Pictures and the Origin of Hurricane Anna", Monthly Weather Review, Vol. 90, pp. 507-513, Dec. 1962.

9. W. R. Bandeen, "TIROS II Radiation Data Users' Manual Supplement", NASA Goddard Space Flight Center, Greenbelt, Md., May 15, 1962.

10. TIROS IV Radiation Data Users' Manual, Goddard Space Flight Center, Greenbelt, Md. - to be published (1964).

ACKNOWLEDGEMENT

The authors are indebted to Mr. W. R. Bandeen, Mr. George W. Nicholas, Mr. Harold P. Thompson, of Goddard Space Flight Center and Mr. L. F. Whitney, Jr., U. S. Weather Bureau for their contributions to the presented analysis work.

FIGURE CAPTIONS

Figure 1 Position of the TIROS radiometer within the satellite.

Figure 2 The effective radiant emittance of the thermal channels of the TIROS III radiometer versus equivalent blackbody temperature.

Figure 3 An empirically-developed correction nomogram for instrumental degradation of Channel 2, TIROS III.

Figure 4 Satellite zenith and nadir angle relationship

a) Scan spot size as a function of zenith and nadir angle of the sensor and the power distribution within the scan spot.
b) Zenith angle and nadir angle relationship.

Figure 5 Cross-section through a detector unit of the TIROS III radiometer and response curve within the field of view.

Figure 6(a) Radiation analysis (Channel 2 data) plotted by hand from a computer listing of the early stage of Hurricane Anna, which was used for the composite in Figure 6(b).

Figure 6(b) Composite analysis of Channel 2 radiation data and a gridded television picture of the early stage of Hurricane Anna.

Figure 6(c) Composite analysis of Channel 2 radiation data and a gridded television picture of the early stage of Hurricane Anna, using the Fujita technique by L. F. Whitney, Jr., U.S. Weather Bureau.

Figure 7 Analysis of Channel 2 radiation data of the early stage of Hurricane Anna, using different resolutions in computer-produced grid print maps (Open mode data only)

a) 0.625° longitude/mesh interval
b) 1.250° longitude/mesh interval
c) 2.50° longitude/mesh interval

FIGURE CAPTIONS (Continued)

Figure 8 Different types of scan modes of the TIROS radiometer generally occurring in one orbit.

Figure 9 Typical example of the data coverage within the open and closed scanning modes for three orbits of TIROS III. Some typical scan lines and the distribution of computer-selected scan spots along these lines are added for demonstration of some characteristic features of scan line geometry.

Figure 10 Analysis of Channel 2 radiation data of the early stage of Hurricane Anna, using different resolutions in computer-produced grid print maps (Open and closed mode data)

a) 0.625^{o} longitude/mesh interval
b) 1.250^{o} longitude/mesh interval
c) 2.50^{o} longitude/mesh interval

Figure 11 Digitized form of the analog signal from Channel 2 during the transition from the single open to closed scanning modes. The numbers along the bottom indicate the minutes and seconds from the beginning of the data. The ordinate is the radiometer output on a relative scale.

Figure 12 Digitized form of the analog signal from Channel 2 during the transition from closed to single open scanning modes. The numbers along the bottom indicate the minutes and seconds from the beginning of the data. The ordinate is the radiometer output in a relative scale.

Figure 13 An example of the scan spot shift at the entrance and exit from the closed scanning mode due to computer program techniques and inaccuracy in spin rate determination, respectively.

FIGURE CAPTIONS (Continued)

Figure 14 Computer-produced grid print map of data population for Orbit 62, TIROS III (2.50° longitude/mesh interval).

Figure 15 Location of scan spots over a tropical cisturbance close to the Philippines, based upon computer listings. (Encircled data in the shaded area were rejected by computer logic in producing the grid print maps).

Figure 16 Radiation analysis (Channel 2 data) over a tropical disturbance close to the Philippines, based upon computer listings. (Data within the grey shaded area were rejected by computer logic in producing the grid print maps)

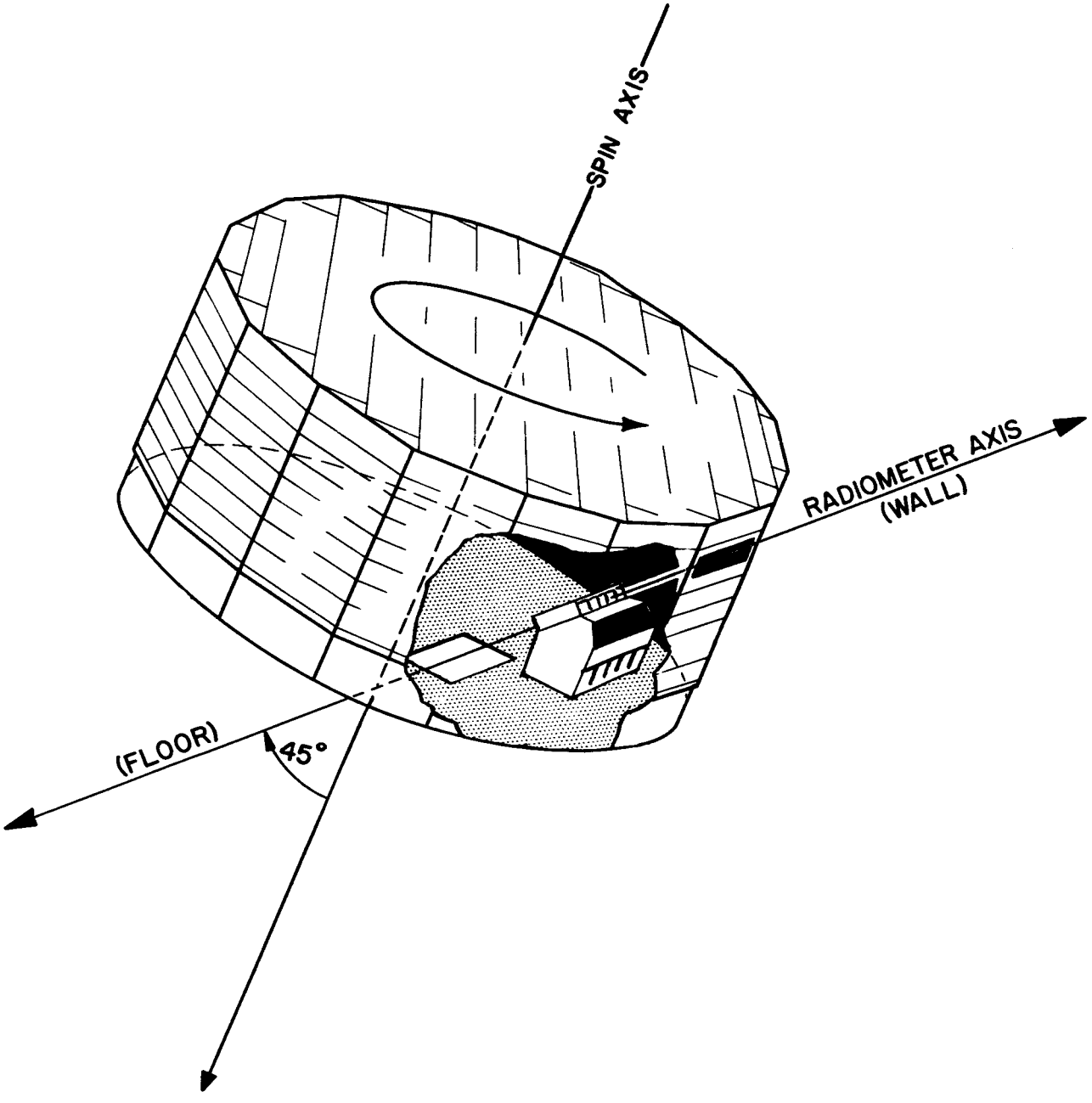

Figure 1

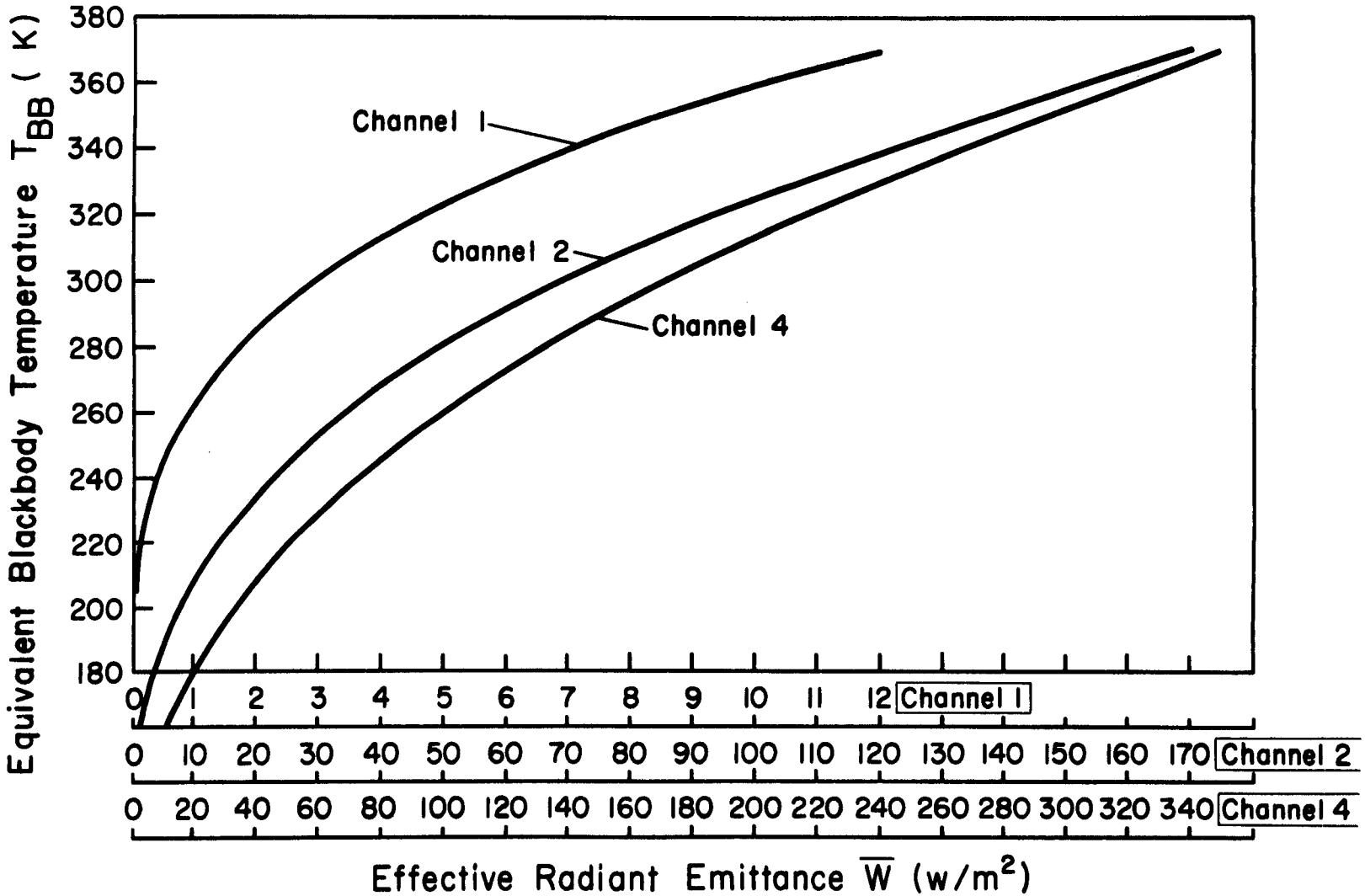
Equivalent Blackbody Temperature T_{BB} (K)
380
360
340
320
300
280
260
240
220
200
180
Channel 1
Channel 2
Channel 4
0 1 2 3 4 5 6 7 8 9 10 11 12 Channel 1
0 10 20 30 40 50 60 70 80 90 100 110 120 130 140 150 160 170 Channel 2
0 20 40 60 80 100 120 140 160 180 200 220 240 260 280 300 320 340 Channel 4
Effective Radiant Emittance $\overline{W}$ (w/m^2)

Figure 2

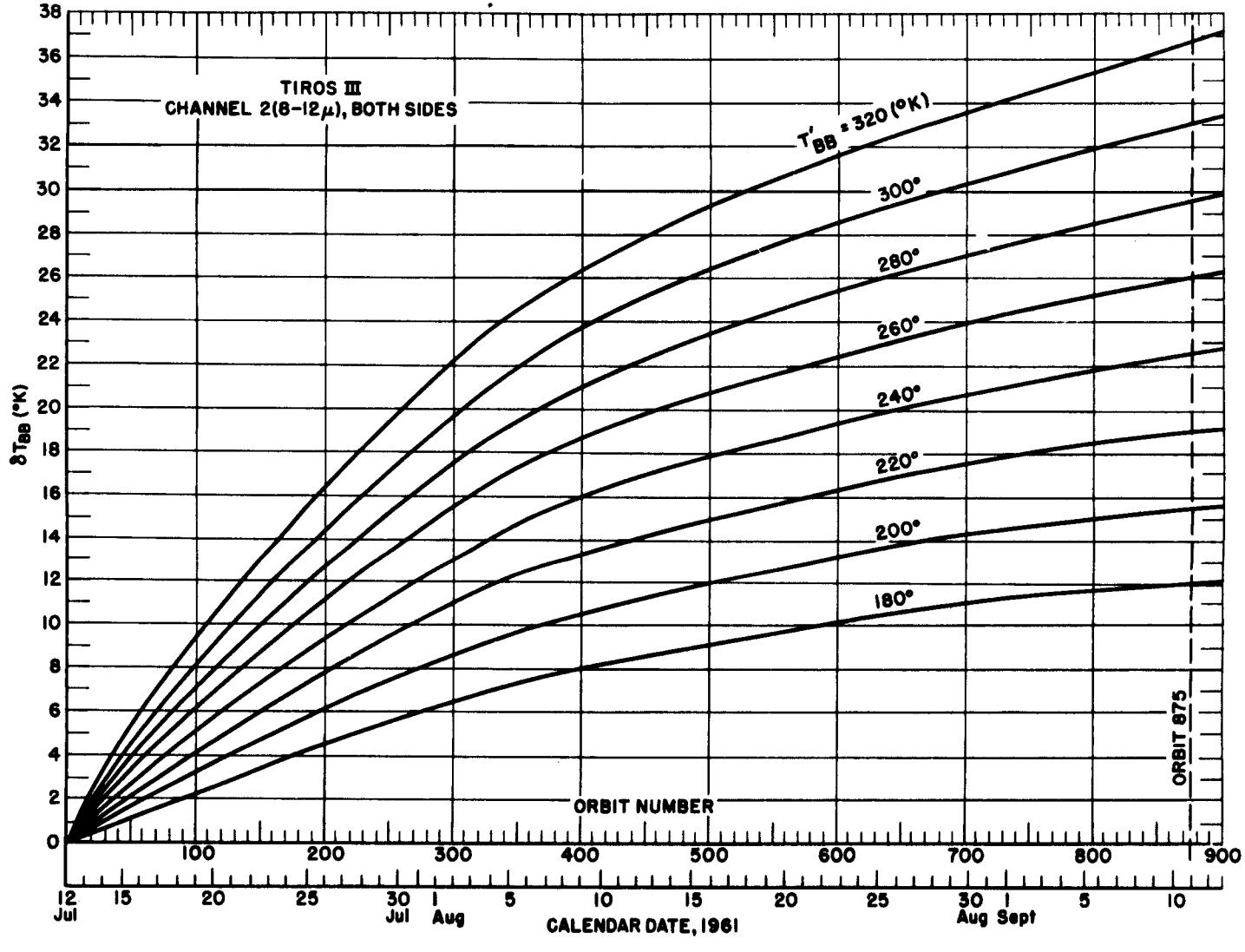
TIROS III
CHANNEL 2(8-12μ), BOTH SIDES
T'BB = 320 (°K)
300°
280°
260°
240°
220°
200°
180°
δTBB (°K)
ORBIT NUMBER
ORBIT 875
CALENDAR DATE, 1961
12 Jul
15
20
25
30 Jul
1 Aug
5
10
15
20
25
30 Aug
1 Sept
5
10

Figure 3

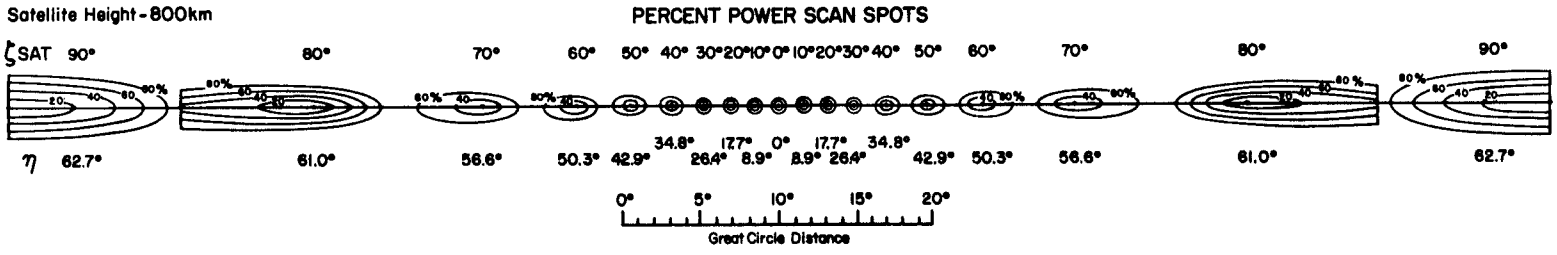
Satellite Height - 800km
PERCENT POWER SCAN SPOTS
ζSAT 90° 80° 70° 60° 50° 40° 30° 20° 10° 0° 10° 20° 30° 40° 50° 60° 70° 80° 90°
η 62.7° 61.0° 56.6° 50.3° 42.9° 34.8° 26.4° 17.7° 8.9° 0° 8.9° 17.7° 26.4° 34.8° 42.9° 50.3° 56.6° 61.0° 62.7°
0° 5° 10° 15° 20°
Great Circle Distance

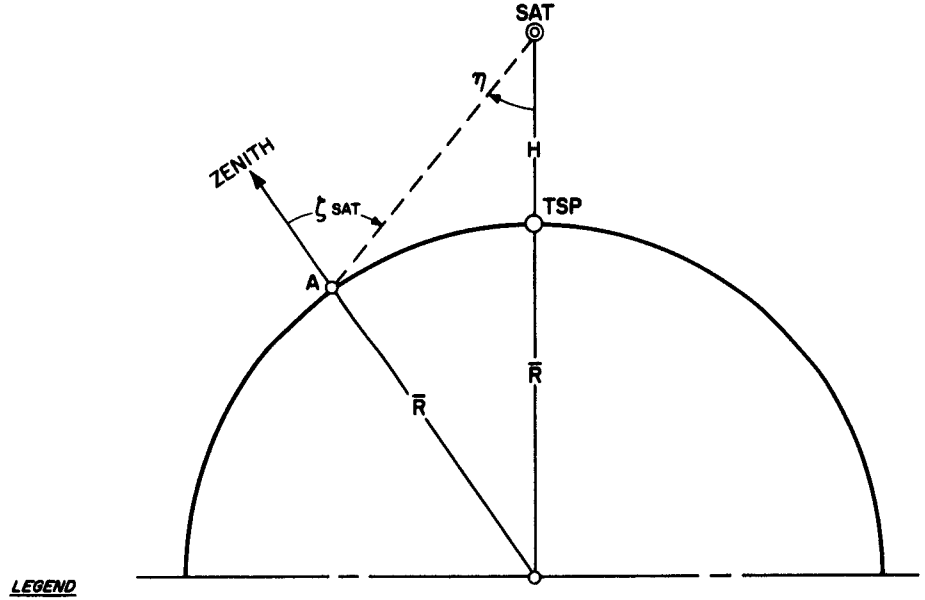
SAT
η
H
ZENITH
ζ SAT
TSP
A
R̄
R̄
LEGEND
ζ SAT – Zenith Angle of Satellite
η – Nadir Angle
TSP – Terrestrial Sub-Satellite Point
sin ζ sat = (R̄+H)/R̄ sin η

Figure 4

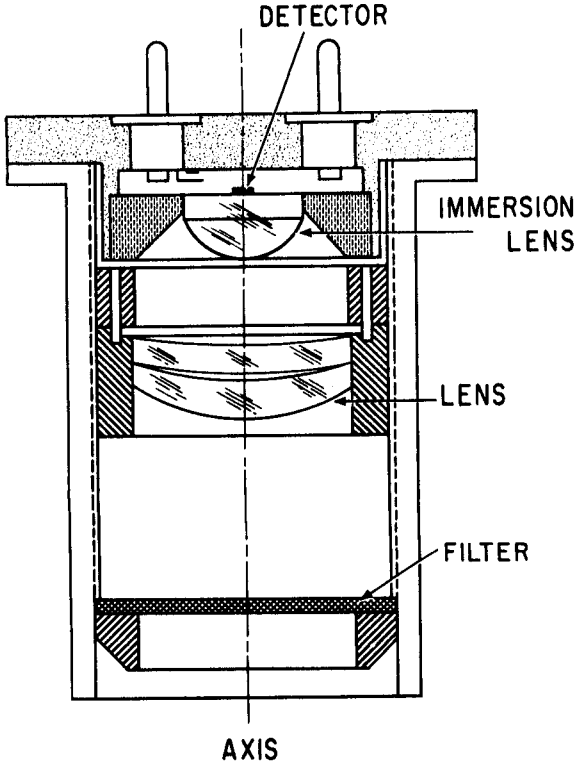
DETECTOR
IMMERSION LENS
LENS
FILTER
AXIS

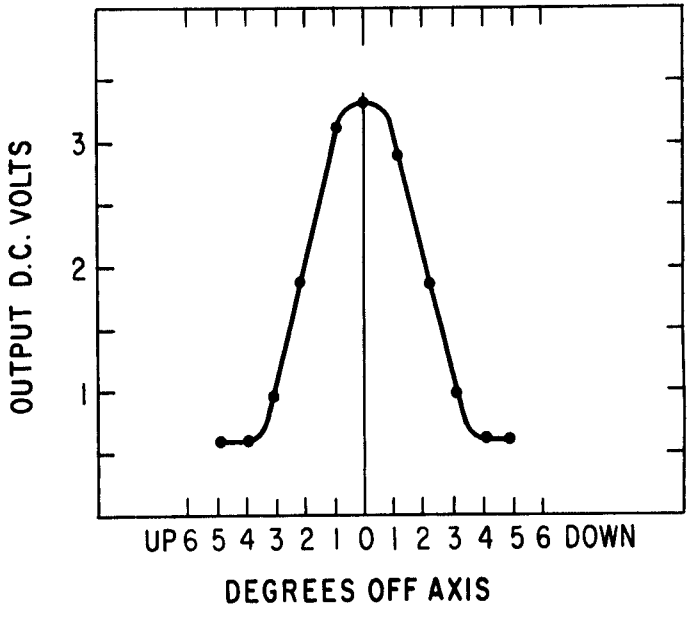
OUTPUT D.C. VOLTS
3
2
1
UP 6 5 4 3 2 1 0 1 2 3 4 5 6 DOWN
DEGREES OFF AXIS

Figure 5

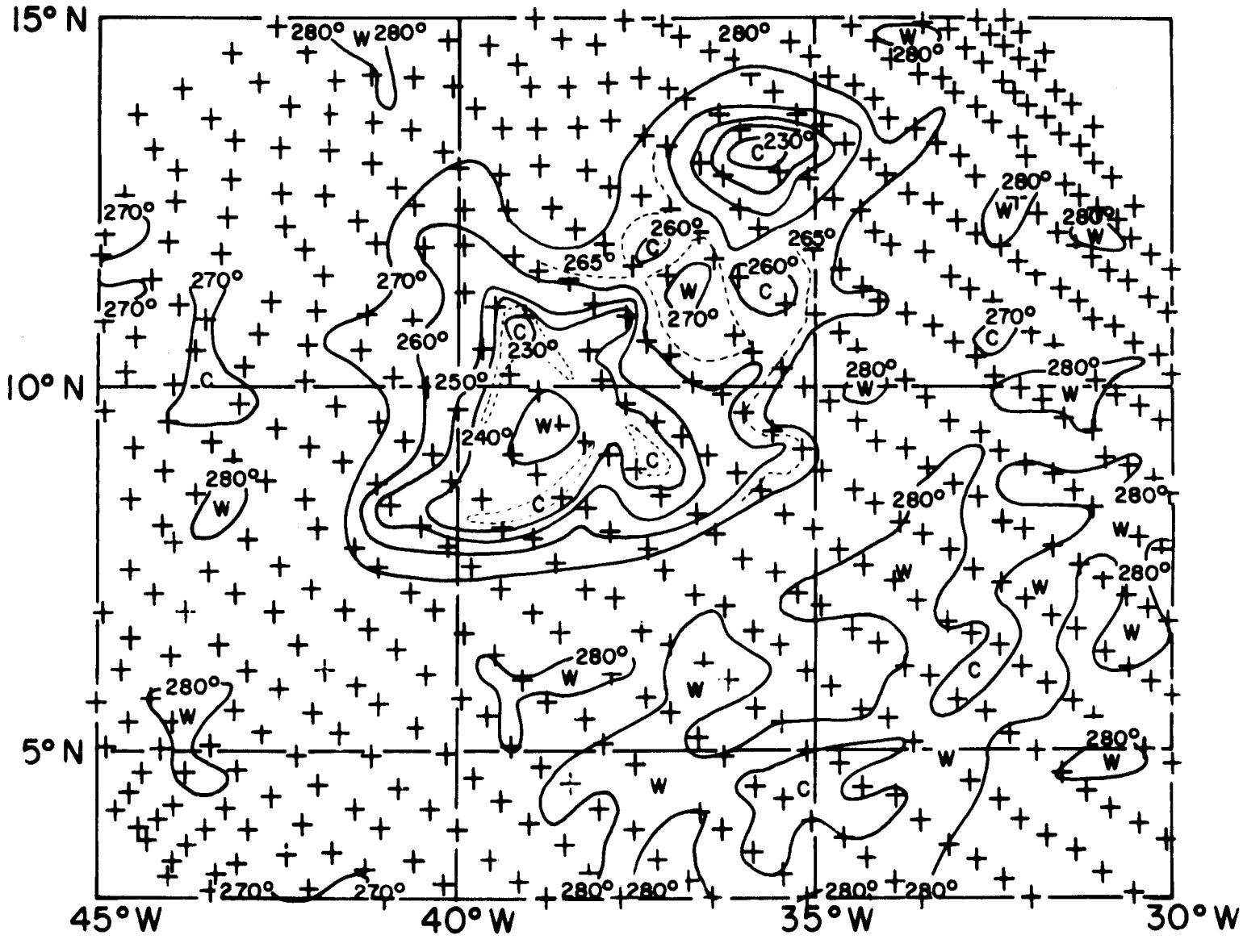

Figure 6(a)

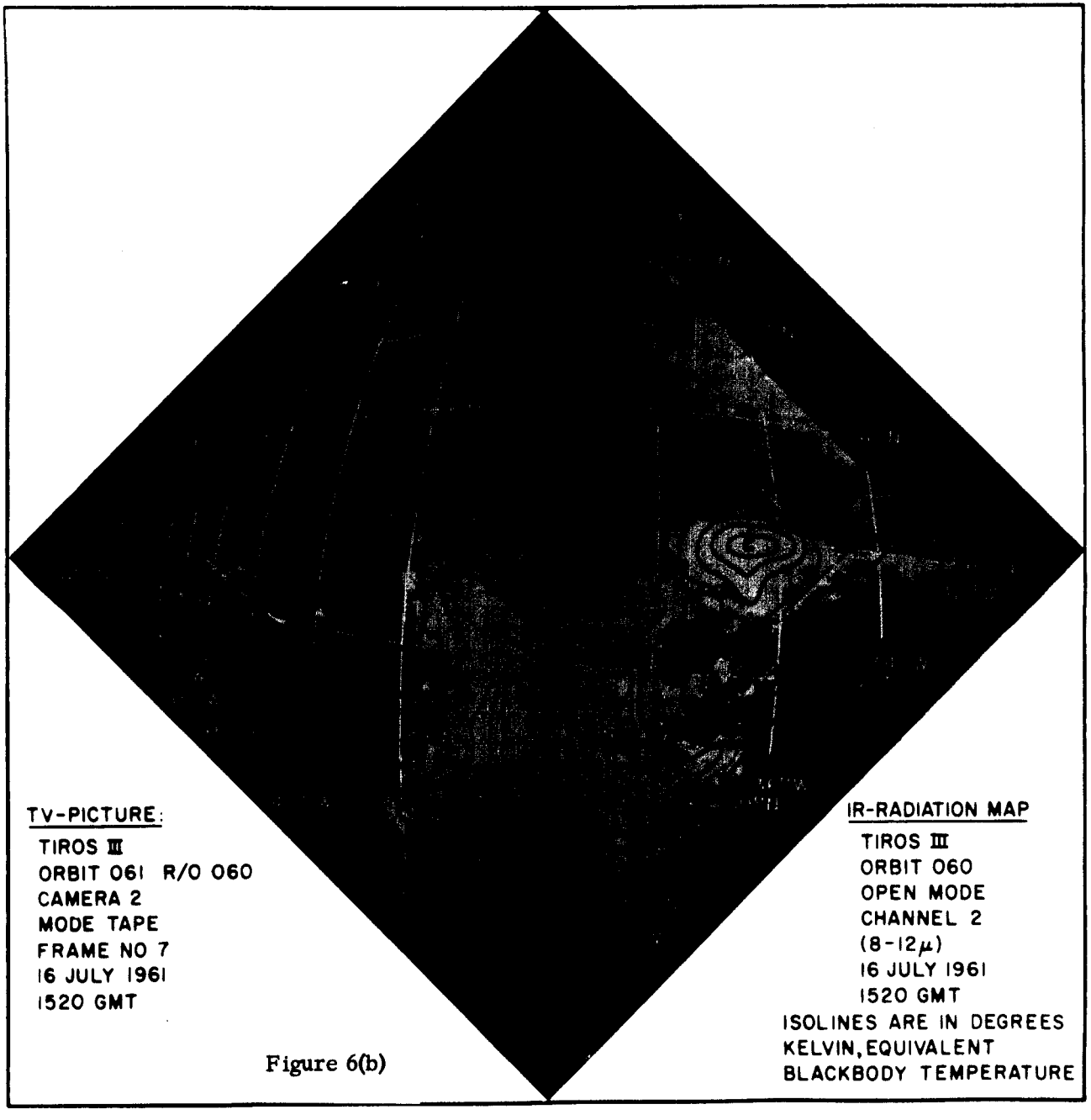
TV-PICTURE:
TIROS III
ORBIT 061 R/O 060
CAMERA 2
MODE TAPE
FRAME NO 7
16 JULY 1961
1520 GMT
IR-RADIATION MAP
TIROS III
ORBIT 060
OPEN MODE
CHANNEL 2
(8-12μ)
16 JULY 1961
1520 GMT
ISOLINES ARE IN DEGREES
KELVIN, EQUIVALENT
BLACKBODY TEMPERATURE

Figure 6(b)

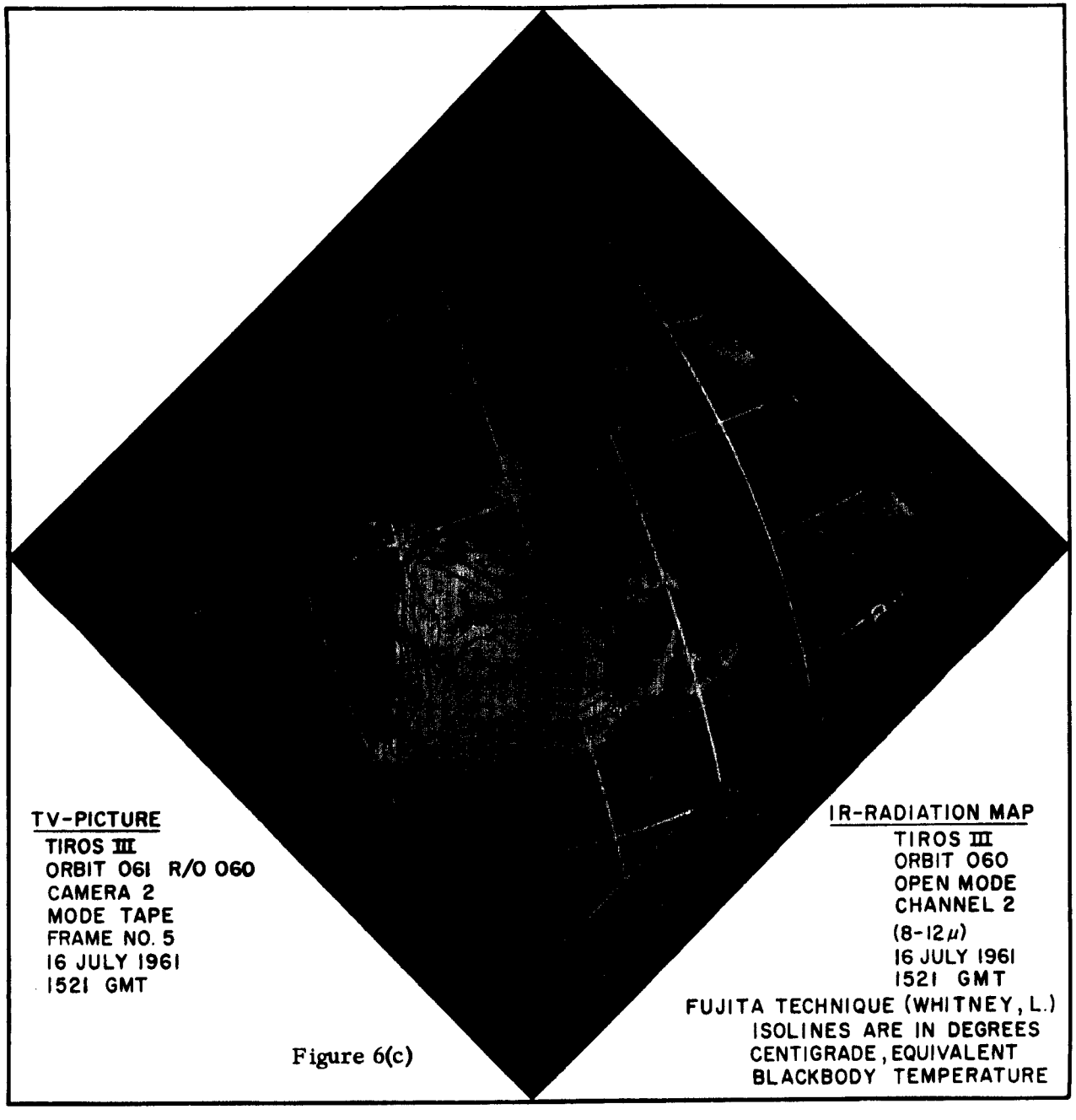
TV-PICTURE
TIROS III
ORBIT 061 R/O 060
CAMERA 2
MODE TAPE
FRAME NO. 5
16 JULY 1961
1521 GMT
IR-RADIATION MAP
TIROS III
ORBIT 060
OPEN MODE
CHANNEL 2
(8-12μ)
16 JULY 1961
1521 GMT
FUJITA TECHNIQUE (WHITNEY, L.)
ISOLINES ARE IN DEGREES
CENTIGRADE, EQUIVALENT
BLACKBODY TEMPERATURE

Figure 6(c)

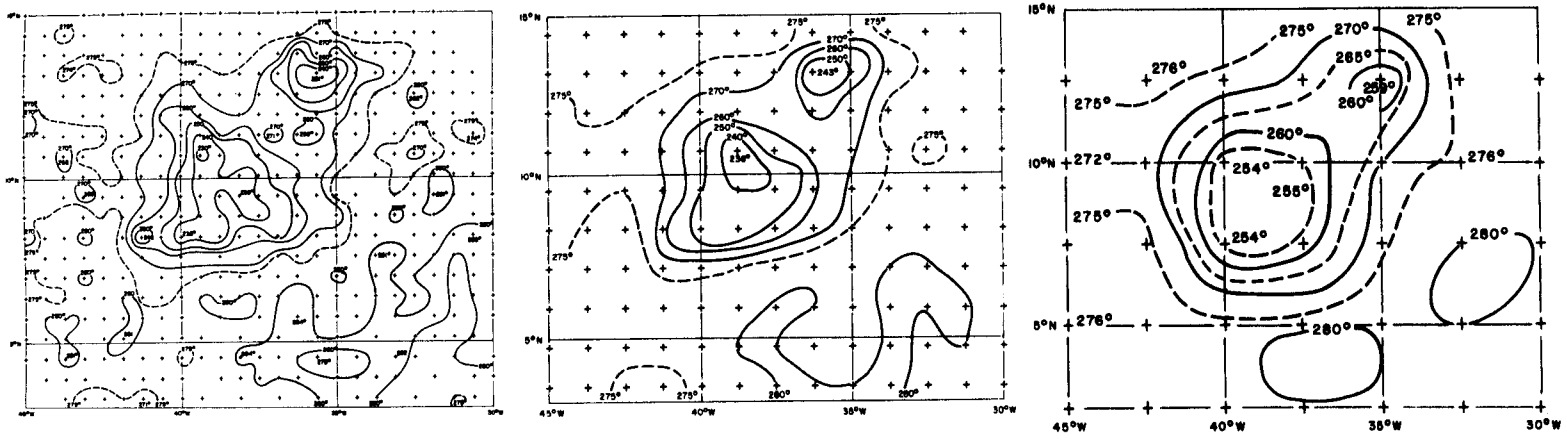

Figure 7(a), (b), (c)

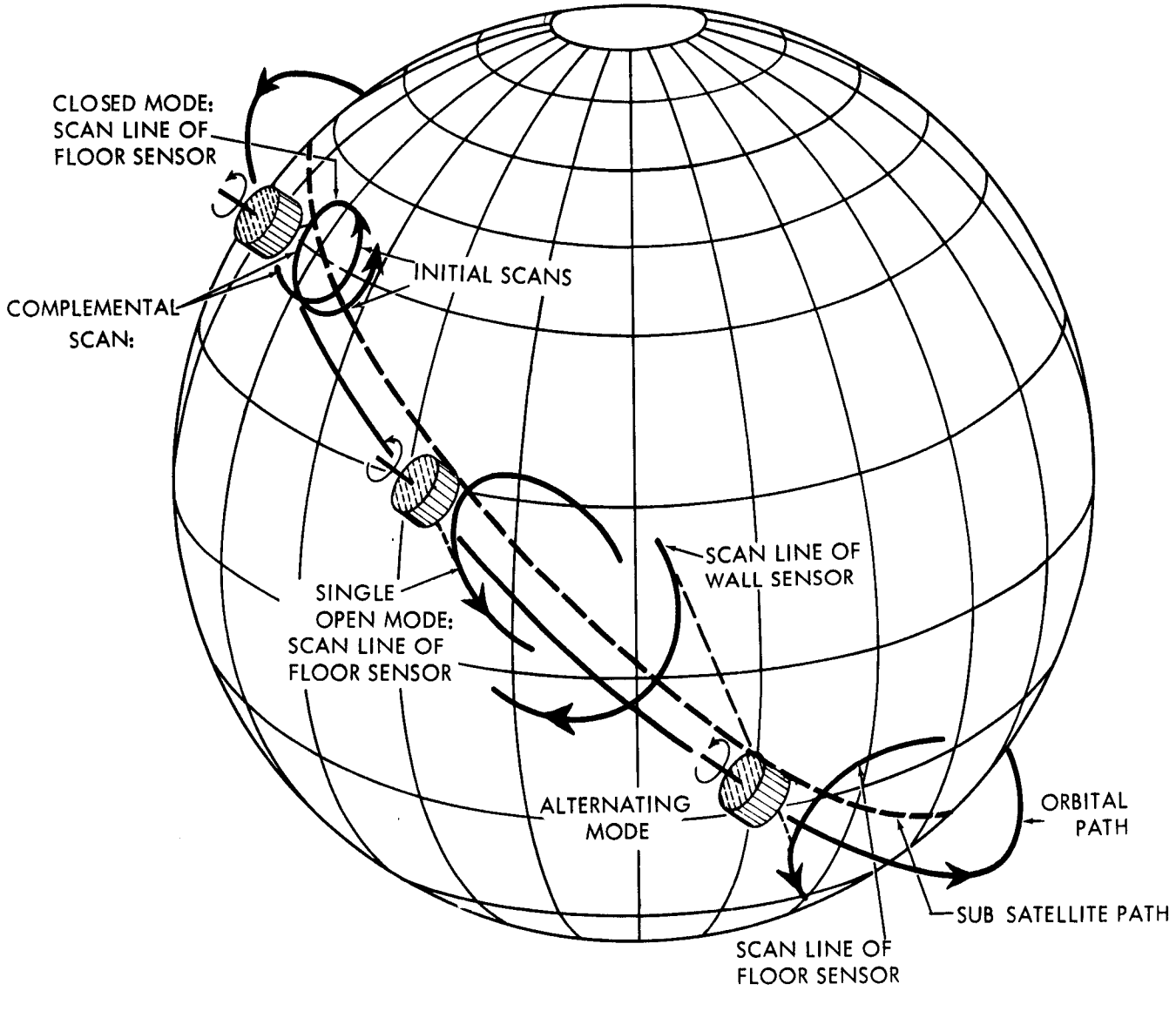
CLOSED MODE:
SCAN LINE OF
FLOOR SENSOR
INITIAL SCANS
COMPLEMENTAL
SCAN:
SCAN LINE OF
WALL SENSOR
SINGLE
OPEN MODE:
SCAN LINE OF
FLOOR SENSOR
ALTERNATING
MODE
ORBITAL
PATH
SUB SATELLITE PATH
SCAN LINE OF
FLOOR SENSOR

Figure 8

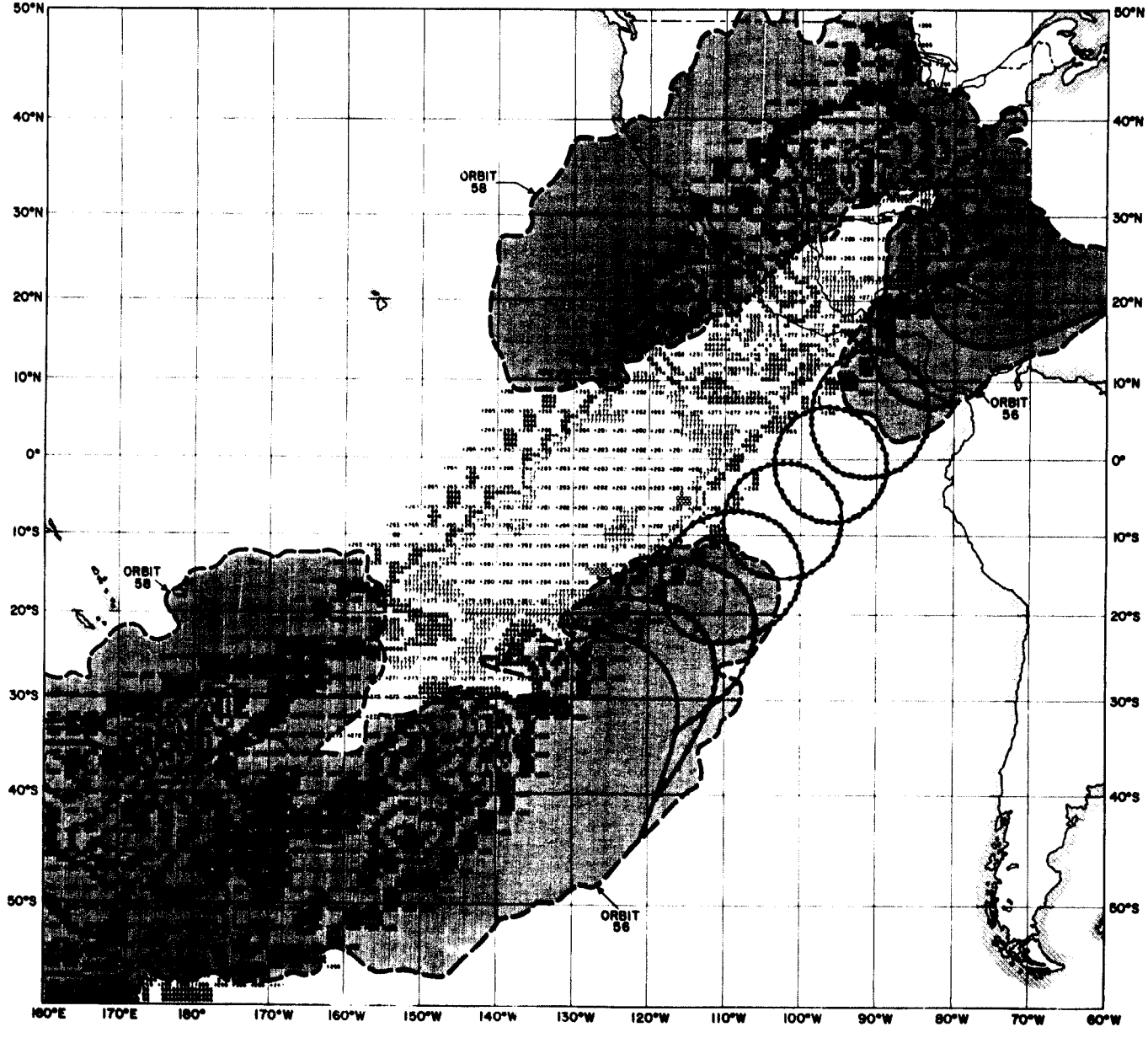
50°N
40°N
30°N
20°N
10°N
0°
10°S
20°S
30°S
40°S
50°S
ORBIT 58
ORBIT 56
ORBIT 58
ORBIT 56
180°E
170°E
180°
170°W
160°W
150°W
140°W
130°W
120°W
110°W
100°W
90°W
80°W
70°W
60°W

Figure 9

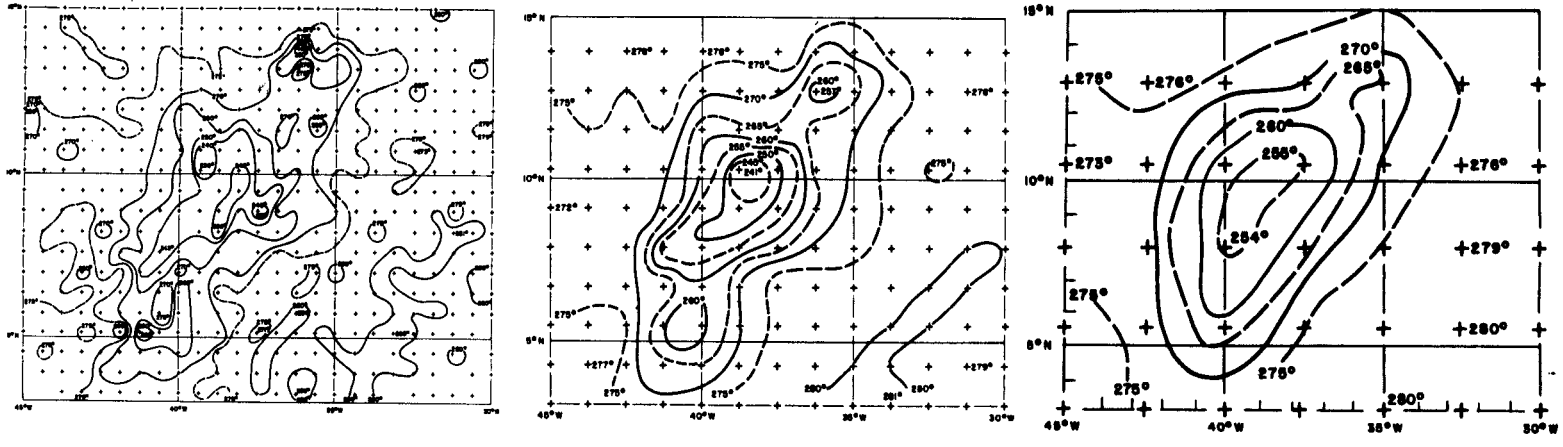

Figure 10(a), (b), (c)

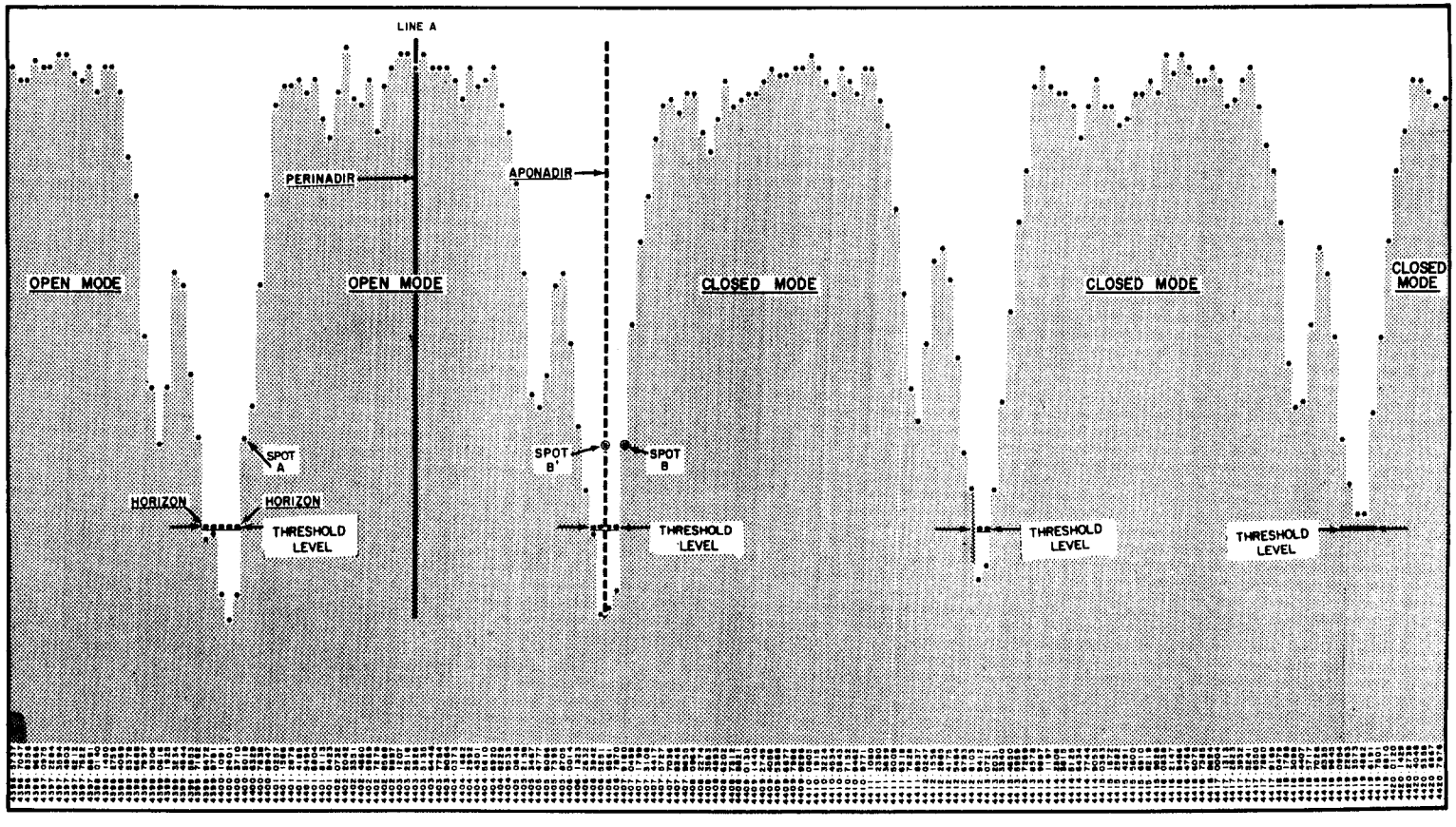
LINE A
PERINADIR
APONADIR
OPEN MODE
OPEN MODE
CLOSED MODE
CLOSED MODE
CLOSED MODE
SPOT A
SPOT B'
SPOT B
HORIZON
HORIZON
THRESHOLD LEVEL
THRESHOLD LEVEL
THRESHOLD LEVEL
THRESHOLD LEVEL

Figure 11

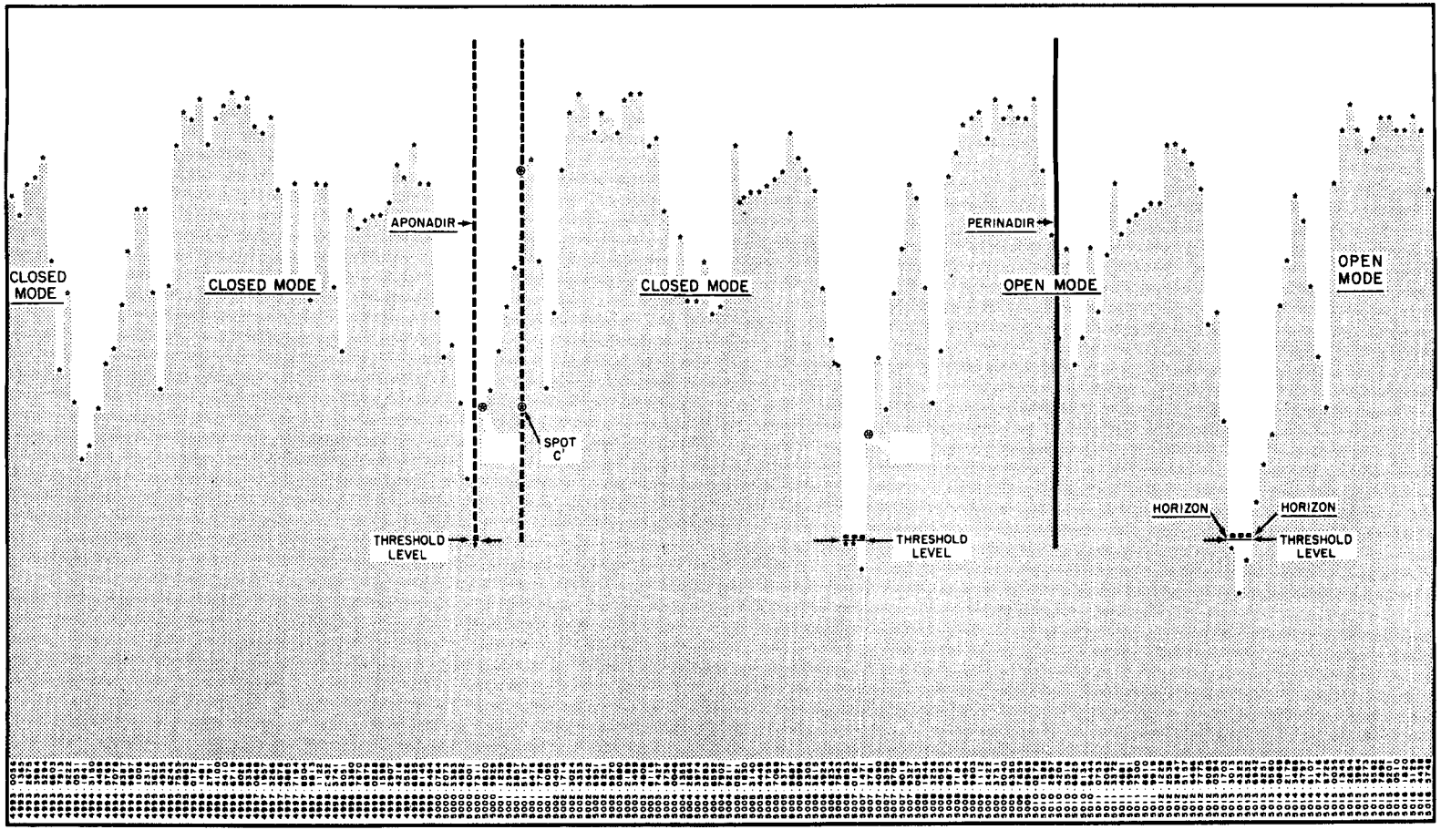
CLOSED MODE
CLOSED MODE
APONADIR
SPOT C'
THRESHOLD LEVEL
CLOSED MODE
PERINADIR
OPEN MODE
THRESHOLD LEVEL
HORIZON
HORIZON
THRESHOLD LEVEL
OPEN MODE

Figure 12

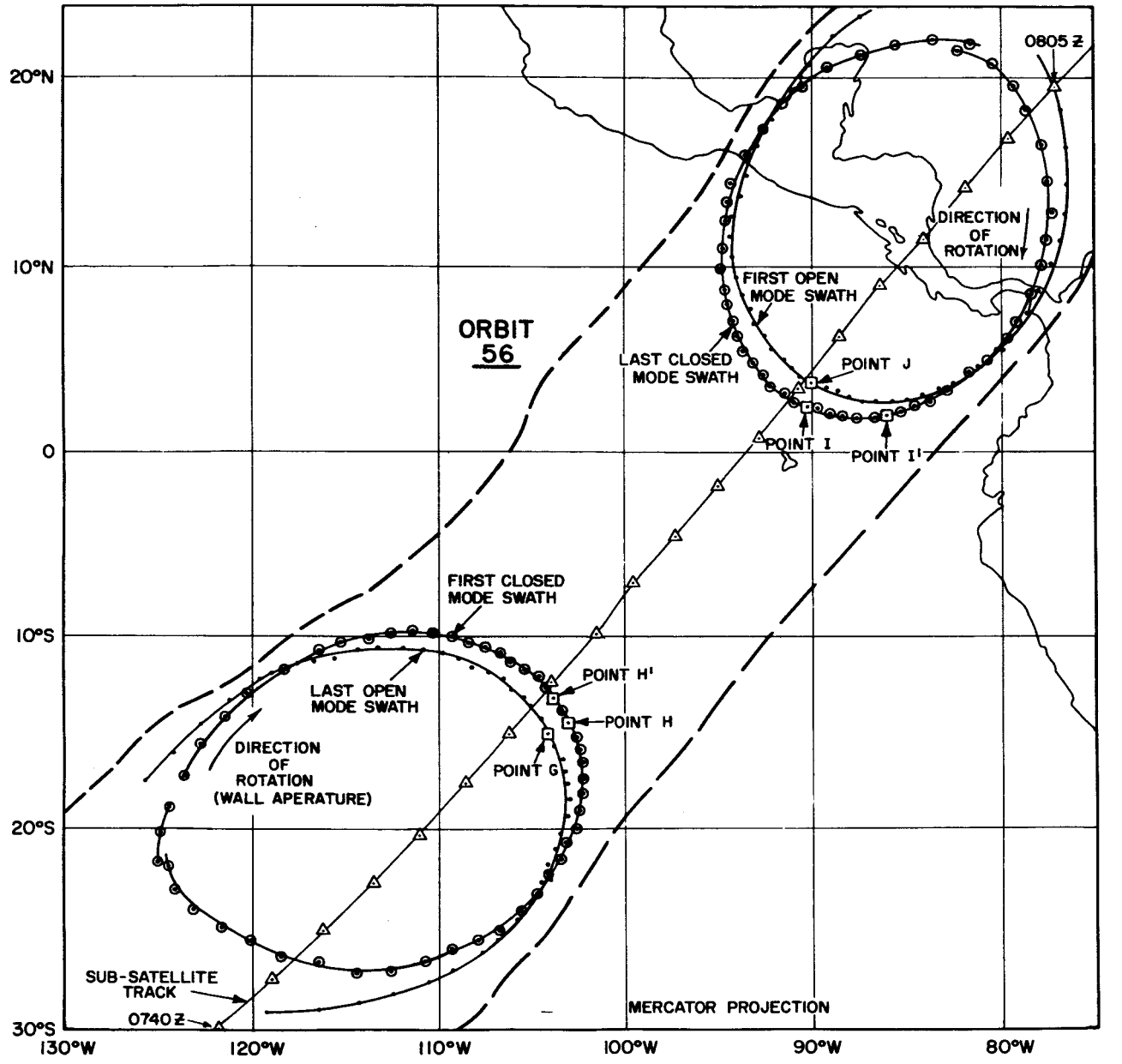
20°N
10°N
0
10°S
20°S
30°S
130°W
120°W
110°W
100°W
90°W
80°W
ORBIT
56
0805 Z
DIRECTION
OF
ROTATION
FIRST OPEN
MODE SWATH
LAST CLOSED
MODE SWATH
POINT J
POINT I
POINT I'
FIRST CLOSED
MODE SWATH
POINT H'
POINT H
POINT G
LAST OPEN
MODE SWATH
DIRECTION
OF
ROTATION
(WALL APERATURE)
SUB-SATELLITE
TRACK
0740 Z
MERCATOR PROJECTION

Figure 13

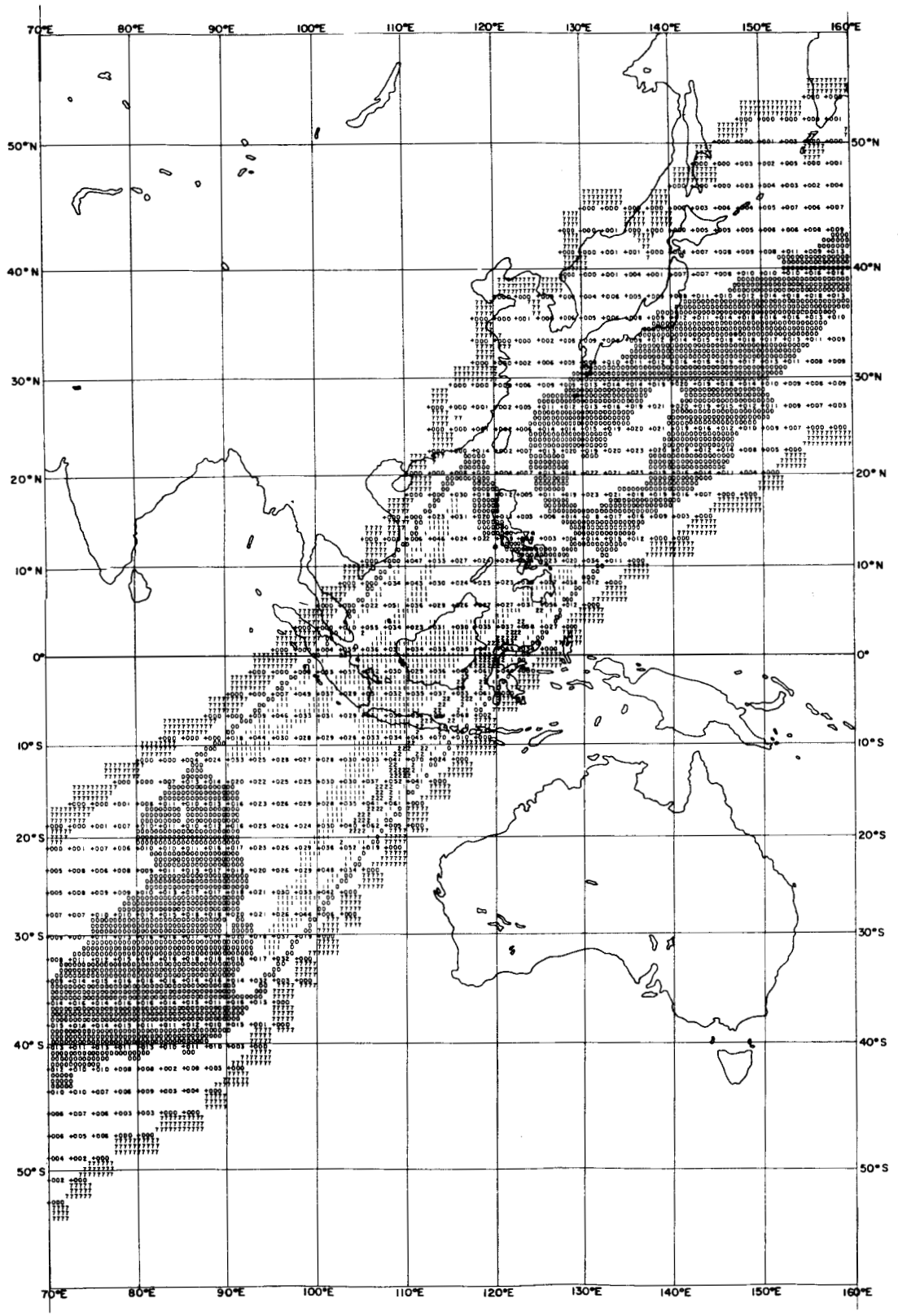
70°E
80°E
90°E
100°E
110°E
120°E
130°E
140°E
150°E
160°E
50°N
40°N
30°N
20°N
10°N
0°
10°S
20°S
30°S
40°S
50°S

Figure 14

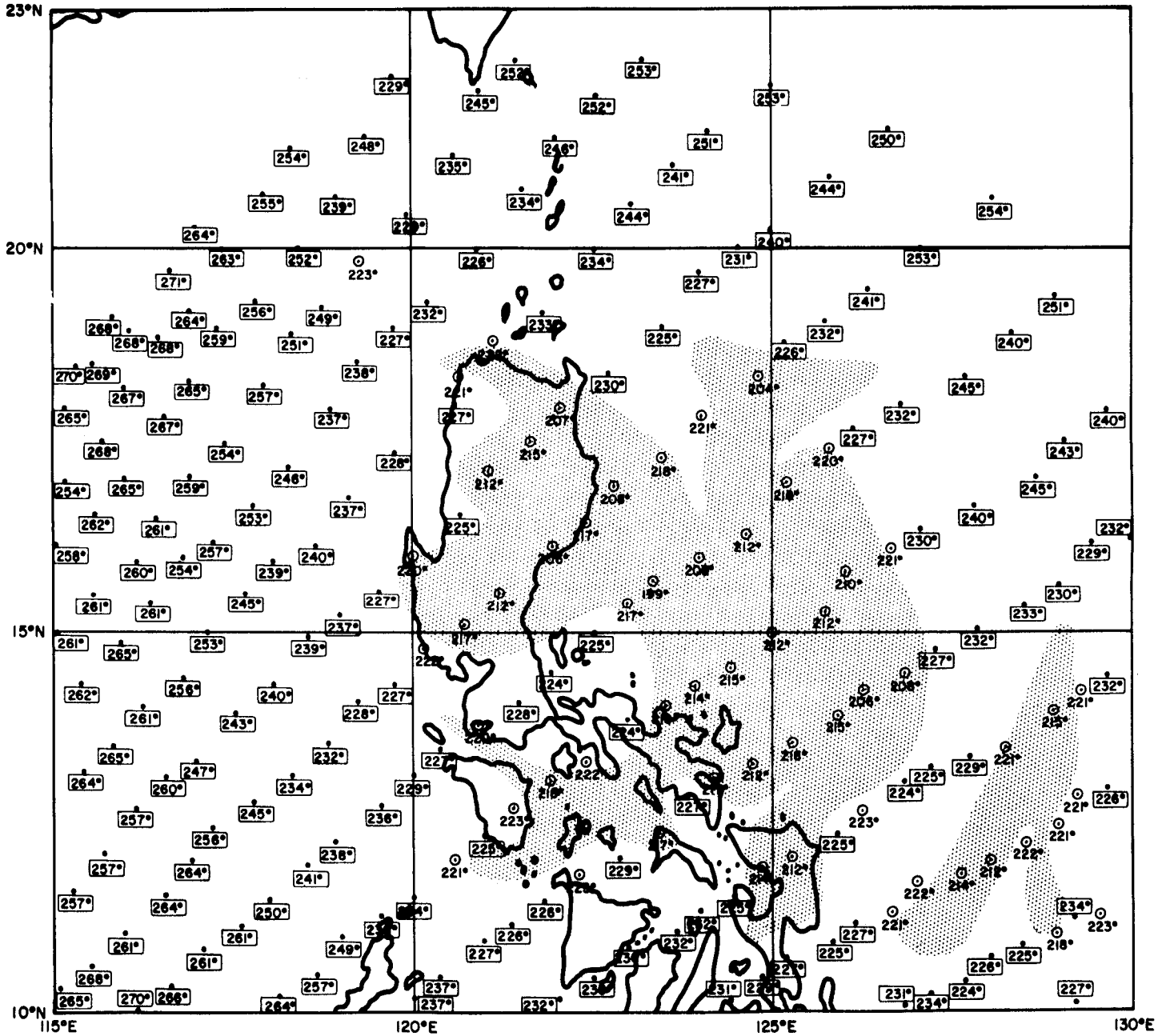

Figure 15

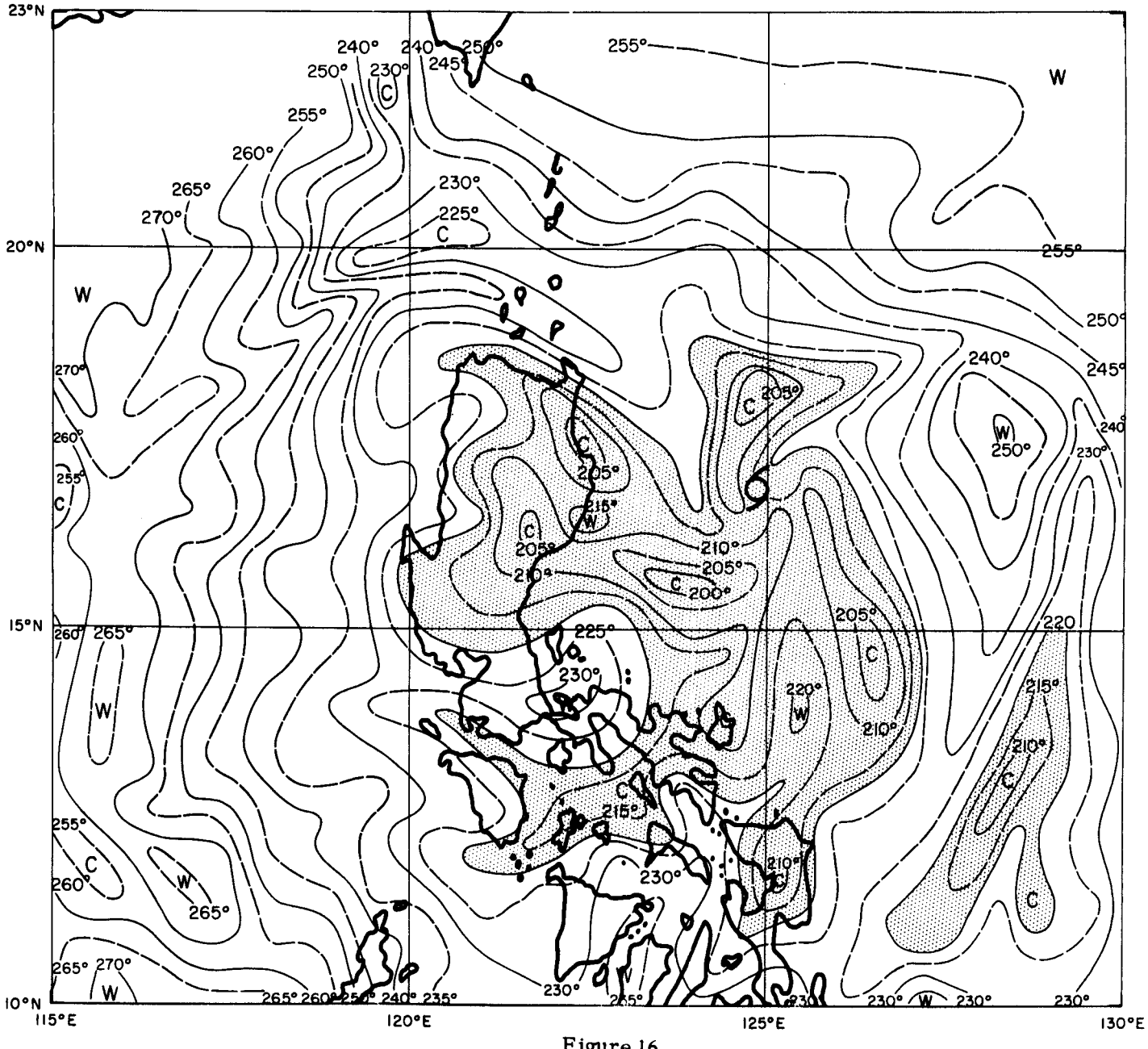
23°N
20°N
15°N
10°N
115°E
120°E
125°E
130°E
W
C
240°
250°
255°
260°
265°
270°
230°
225°
245°
205°
215°
210°
200°
220°
235°

Figure 16